Egyptian Knowledge Bank
https://ijmti.journals.ekb.eg/

International Journal of Materials Technology and Innovation
Volume 3, Issue 2 (2023), pages 19-29

Online ISSN 2682-4299

Effect of heat input on weldability of low nickel high manganese stainless steel

Mohamed H. Abd-Allatif[1], Ahmed M. Elsabbagh[1], Hossam A. Halfa[2], Ahmed A. Eid[3]

[1] Professor at Mechanical Design and Production Eng. Dept., Ain Shams University, Cairo-Egypt
[2] A. Professor at Steel Technology Dept., Central Metallurgical R & D Institute, Cairo-Egypt.
[3] Production Engineer at Chinese Co., 6th October City, Egypt.

* Corresponding author: E-mail:ammer5599@gmail.com, Tele, +201279520023-+2011027977544.

Received 7 March 2023
Accepted 8 June 2023
Published 30 June 2023

Abstract

The effect of heat input on the microstructure and mechanical properties of low nickel-high manganese stainless steel welded using a shielded metal arc was investigated. Six samples divided equally into two groups that represented the two distinct degrees of heat input were conducted: low heat (128 J/mm- 139 J/mm-165 J/mm) and high heat (182 J/mm -207 J/mm- 225 J/mm), respectively. These groups were subjected to microstructural analyses and tensile tests to see how heat input affected their joints' mechanical characteristics and microstructure evolution. In the second group, the high value of the ultimate tensile strength (UTS) was found in the case of the high-heat input (182 J/mm) sample. Macrostructure observations were made at the melting zone for each sample. In the case of low heat input formation, partial penetration was observed. However, in the case of high heat input formation, full penetration was observed in all samples treated to the various heat inputs. No defects, such as cracks or voids, were found. In addition, it was observed by increasing heat inputs that the average inter-dendritic spacing in the weld zone increased, which plays a significant role in the observed changes in the tensile characteristics of the welded samples.

Keywords: 200-series austenitic stainless steel, shielded metal arc welding, Ferrite-scope, non-destructive test, tensile strength, microhardness, microstructure evolution

1. Introduction

Nickel is one of the essential elements in austenitic stainless-steel alloys. Nickel works as an austenitic stabilizer. Because of the price fluctuation in nickel, lack of stock, and essential role in stainless steel alloys, it was necessary to search for economic alternatives [1, 2].

Manganese can be used as a substitute for nickel. Although nickel is a more vital austenitic stabilizer than manganese, manganese plays an essential role in increasing nitrogen's solubility, which can improve corrosion resistance. Furthermore, nitrogen can play a crucial role as an austenitic stabilizer and increases work hardening and strength without disturbing the toughness properties of the steel. The mentioned properties may be driven by better energy absorption and weight reduction leading to higher impact resistance [3, 5].

On the other hand, adding copper traces can reduce nitrogen content. Copper can stabilize the austenite phase; hence softer manganese austenitic grades can be obtained. Recently, high-manganese low-nickel austenitic stainless steel and 200 new European-grade austenitic chromium-manganese stainless steel were produced [6, 8].

Compared to other welding processes, shielded metal arc welding (SMAW) is an exceptionally commercially appealing welding process [9, 10], like tungsten-inert gas (TIG) welding. Shielded metal arc welding (SMAW) is a frequently used fabrication technique for bonding stainless steel. It was necessary to establish a process of filler materials and

IJMTI vol. 3, issue 2 (2023) 19-29 https://doi.org/10.21608/IJMTI.2023.196160.1078

manufacture for the newly developed inexpensive high manganese-low nickel austenitic stainless steel [11, 12]. A new alloying design was necessary since the new stainless steel was being developed.

SMAW is a primarily used technique to join the austenitic St. St. SMAW is always challenging due to differences in composition and physical and thermal properties, as it is associated with many defects, such as solidification cracking, porosities, and micro-segregation [13].

Solidification cracking affects the properties of the weldment majorly. In austenitic stainless-steel weldment, ferrite plays a crucial role in solidification cracking, and controlling its volumetric fraction can prevent such defects [14].

Therefore, it becomes vital to identify the welding process parameters which result in an optimum volumetric fraction of ferrite and thus give the best mechanical and corrosion properties and can have a longer life. Hence, the main objective of this paper is to study the welding behavior of the cheapest austenitic stainless (200) series and help to determine the optimum parameters that achieve good mechanical properties.

During the SMAW process, it is well-known that the welding current, denoted by {I}, has the most significant influence on the heat input and, consequently, on the choice of filler material for particular base materials [15]. The welding current influences mechanical and microstructural qualities by modifying the heat-affected zone (HAZ) width and the weld pool's morphology [16, 17].

200-series austenitic are typically used to replace types 304 and 301 as well as Carbon (Chrome-Manganese) Steels mainly for indoor use for low corrosion applications at room temperature, Furniture; Bins; Cookware & Serving Bowls; Window Channel Spacers; Safety Shoes (mid-sole protector); Deep drawn kitchen equipment – e.g., Cookware & Sinks; Hose Clamps; Trailer Frames; Industrial Strapping; Railway Rolling Stock. There is also grade 201LN for welded constructions, structural uses, and low-temperature applications. Examples include sides & roofs of trains, liquified gas storage vessels, structural members/chassis of railway rolling stock, trucks & trailers, and coal handling equipment.

The primary goal of this work is to evaluate the effect of heat input on the microstructure and its effect on the mechanical properties of welded low nickel-high manganese stainless steel.

2. Experimental Procedure

High manganese, low-nickel austenitic stainless steel was purchased from the regional market as a rolled sheet (2000*1000*2 mm). Table 1 shows the chemical composition of the studied steel determined by an optical emission spectrometer.

Table.1 Chemical composition of the examined austenitic stainless steel

Sample	Chemical Composition, wt.%										
	C	Cr	Ni	Mn	Si	P	S	Mo	Al	N	Cu
Low nickel St. St.	0.104	12.6	1.35	10.3	0.362	0.033	0.003	0.01	0.003	0.0264	0.294

Twelve Identical samples were sliced with a mechanical saw with dimensions (100 lengths, ×50 width × 2 thickness mm).

The samples were cut in the rolling direction. The samples were cleaned from grease and lubricant oil by immersion in a hydrochloric acid diluted by water (1:1000) for two seconds, then washed in water and immediately immersed in ethyl alcohol. The samples were then dried by using an air drier. The SMAW process uses a welding machine type (APT-Solda-280 A). The consumable electrode E308L (AWS A5.4) of a diameter of 2 mm was used in the present study for making a weld joint. The chemical analysis of this electrode is shown in Table 2.

Table. 2 Chemical composition of Electrode (E308L)

Electrode No.	Electrode Composition Wt. %					
	C	Cr	Ni	Mo	Mn	Si
E308 L	0.03 Max	19.5 -22	9.0- 11.0	0.75 Max	1.0- 2.5	0.30- 0.65

IJMTI vol. 3, issue 2 (2023) 19-29 https://doi.org/10.21608/IJMTI.2023.196160.1078

The welder adjusted the welding machine and fixed each two samples in the jig. The welding parameters (current, volt, and time) were measured during the welding process using (a clamp ampere, voltameter, and stopwatch). All joints were welded similarly in a flat welding position. Distortion control must be considered when designing weldments of these alloys because the coefficient of thermal expansion of austenitic stainless steel is high. Robust jig and fixture were designed to hold parts in place during welding, as shown in Fig. 1.

Fig. 1 Designed fixture to hold the samples during the welding process

Six conditions of different heat inputs were selected experimentally built on sheet thickness and electrode diameter that achieved welding joint performance, as shown in Table (2), and the heat inputs were estimated using the empirical equation given below (1) [18,19].

$$Q = \eta * \frac{VI}{v} \quad (1)$$

Where,

{V} is arc voltage in volts,
{I} is welding current in amperes,
{v} is welding speed in mm/s.
{η} Arc efficiency = 0.7

The electrode effect causes a shift in chemical composition in the samples after comparable welding in a flat position with various heat inputs. The schematic section represented in Fig. 2 shows the formed welding zones. From these welded sheet plates, tensile test samples were machined, matching ASTM E-8M standards [8]. Macro and microstructural examinations, as well as microhardness samples, were cut utilizing the wire-cut EDM technique. The schematic demonstration of the obtained specimens is represented in Fig. 3.

Table. 3 Investigated welding parameters variations.

Code	Current (A)	Voltage (v)	Velocity (mm/s)	Heat input/unit length(J/mm)
1	31	19	3.2	127.8
2	40	20	4.0	139.4
3	50	23	4.9	165.0
4	60	24	5.6	181.4
5	70	26	6.2	207.2
6	80	27	6.7	225.3

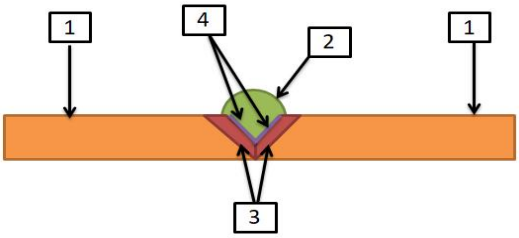

Fig. 2 Schematic section of the formed welding zones: {1} Base metal, {2} Weld zone, {3} Heat-affected zone (HAZ), and {4} Fusion line.

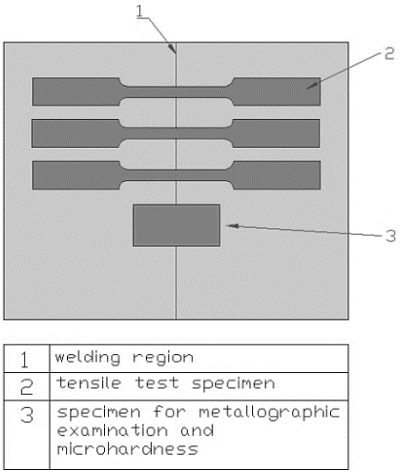

Fig. 3 Schematic demonstration of specimens attained within the welded plate for mechanical properties and metallographic examination

IJMTI vol. 3, issue 2 (2023) 19-29 https://doi.org/10.21608/IJMTI.2023.196160.1078

The 8 mm part was disposed of with wire-cut EDM from both sides of investigated welded steel plates to avoid the starting and end effects of the welding heat. The tensile specimen of Dimension (100 × 10 × 2 mm^3) was removed from the investigated welded steel plates in the crossways direction to determine the ductile tensile properties of the welded joint. All tensile test specimens were prepared and fractured during the tensile testing by "The Shenzhen WANCE testing machine" with a limit load capacity of 30KN.

A 30 × 10 × 2 mm^3 sample was used for macrostructure, metallographic examination, and microhardness. For all six weld steel plates, a sample was cut from the transverse route of the weld in the center of the weld direction.

The preparation of the microstructure sample was coarse ground on emery paper, hot mounted, ground on a series of emery paper, polished, and electro-etched in 20 Wt.% sodium hydroxide solution with 3-volt dc for 20 seconds.

Vickers microhardness tester was used with 100 g of indentation load dwell time of 10 s at room temperature. For each sample, different measurements were taken in all cross-sections, which covered formed welded zones.

3. Results and Discussion

3.1 Phase Identification

Schaeffler diagram was used to specify the phases of the investigated high manganese low-nickel austenitic stainless steel in as-received condition. Nickel equivalent (Ni_{eq}) and Chromium equivalent (Cr_{eq}) were calculated using the given equations below the value of alloying elements in wt, % [20].

$$Cr_{eq}=Cr+2(Si) + 1.5(Mo) + 5(V) + 5.5(Al) + 1.75(Nb) + 1.5(Ti) + 0.75(W) \quad (2)$$

$$Ni_{eq}= (Ni) + (Co) + 0.5(Mn) + 0.3(Cu) + 25(N) + 30(C) \quad (3)$$

The relationship between Ni and Cr equivalent (Cr_{eq} as abscissa and Ni_{eq} as coordinate) was determined utilizing Schaeffler diagrams. The Schaeffler diagram was then used to locate the values of Ni_{eq} (10.53) and Cr_{eq} (13.87). Fig. 4 depicts the examined stainless steels theoretically determined phase composition, consisting of 45% austenite and 55% martensite. The optical microscope depicted in Fig. 5 verified the Schaeffler diagram-detected phases.

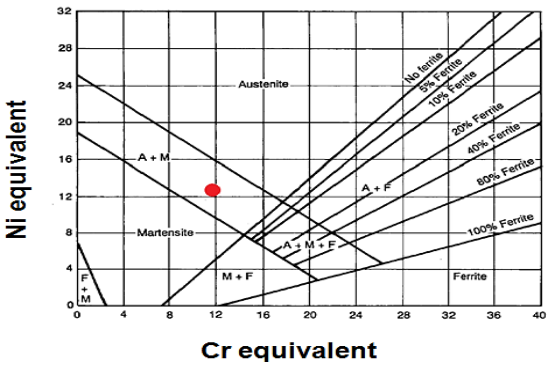

Fig. 4 Schaeffler diagram Cr_{eq} & Ni_{eq} of the investigated steel and the corresponding phase location

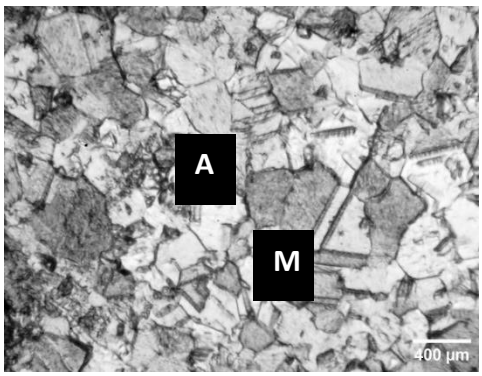

Fig. 5 Optical micrographs show the microstructure of the austenitic stainless steel (A-austenite, M-Martensite).

3.2 Macrostructure investigation of welded samples

The preparation of macrostructure samples was carefully done. The samples were cut carefully using wire cut EDM; the specimens were coarsely ground, hot mounted in bakelite, ground, polished, and etched to appear the formation of welded zones.

Fig. 6 shows typical micrographs of low-nickel high-manganese austenitic stainless-steel specimens welded using different heat input parameters. The formed welded zones have been viewed in the macrographs. Partial and complete penetrations were observed. There are no imperfections in welded joints, such as cracks, voids, etc.

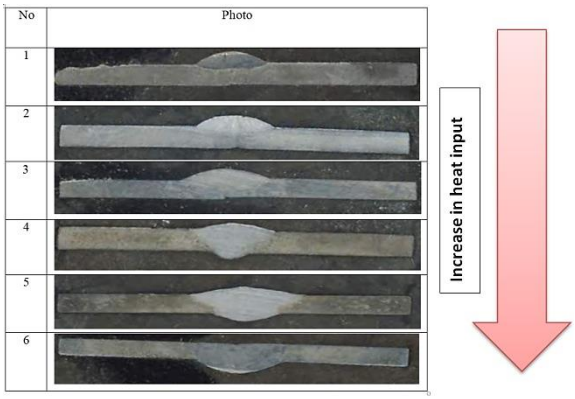

Fig. 6 Macrostructure of welded joints

3.3 Solidification mode and ferrite-number measurements.

The chemical composition of the base metal and electrode determines the solidification mode in the fusion zone according to Eqs. (4) & (5) [21]:

$Cr_{eq}=Cr+Mo+0.7Nb$ (4)

$Ni_{eq}=Ni+35C+20N+0.25Cu$ (5)

The solidification mode can be determined by Creq/Nieq using the WRC-1992 diagram and is divided into four cases [20]:

1-Austenite mode (A):$Cr_{eq}/Ni_{eq}<1.25$ (6)

2-Austenite – Ferrite mode (AF):

$1.25<Cr_{eq}/Ni_{eq}<1.48$ (7)

3-Ferrite – Austenite mode (FA):

$1.48<Cr_{eq}/Ni_{eq}<1.95$ (8)

4-Ferrite (F) mode :$Cr_{eq}/Ni_{eq}>1.95$ (9)

In this study, the calculated value of Cr_{eq}/Ni_{eq} is 2.26; therefore, the solidification mode is found to be ferrite mode (F) (as per Eq 9).

A Ferrite scope was used to detect ferrite in the stainless steel. The Ferrite scope upon probe was placed on the specimen's surface to obtain the exact ferrite content. The ferrite number reading was displayed automatically and memorized in the instrument software.

The ferrite content in the fusion zone in terms of ferrite number (an average of ten readings was taken along the welding line) was measured by ferrite-scope diagrammatically, as shown in Fig. 7. It can be observed that ferrite content in the fusion zone increased with increasing heat input.

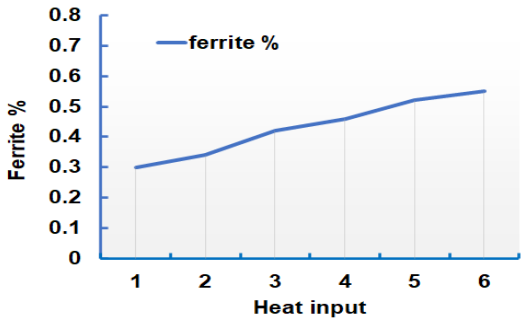

Fig. 7 Effect of Heat input variation on ferrite number measurements

3.4 Effect of heat input on heat-affected zone

Increasing heat input in the welding process causes different thermal cycles in formed welding zones, affecting the heat-affected zone (HAZ) dimensions, mechanical properties, and morphology, as shown in Fig. 8a and b.

The width of the sensitization zone calculated the effect of heat input on HAZ, the heat-affected zone's width, and the true HAZ's (sensitized zone plus heat-affected zone), as shown in Fig. 8a. Table 4 indicates that the breadth of these zones was calculated using an image analyzer.

Increasing the heat input value decreased the cooling rate significantly, and sufficient time was available for grain growth. This grain coarsening leads to a significant increment in the sensitized zone (SZ) and HAZ; hence, the true HAZ increased subsequently for higher heat inputs and quantitatively, as shown in Fig. 9 and 10.

Table. 4 Heat inputs effect on the measurement of HAZ, SZ, and true HAZ

No.	SZ (µm)	HAZ (µm)	True (HAZ) (µm)
1	28.33	31.04	59.37
2	63.19	48.04	111.03
3	73.42	64.62	138.04
4	91.43	87.61	179.04
5	114.27	109.58	223.85
6	133.62	124.31	257.93

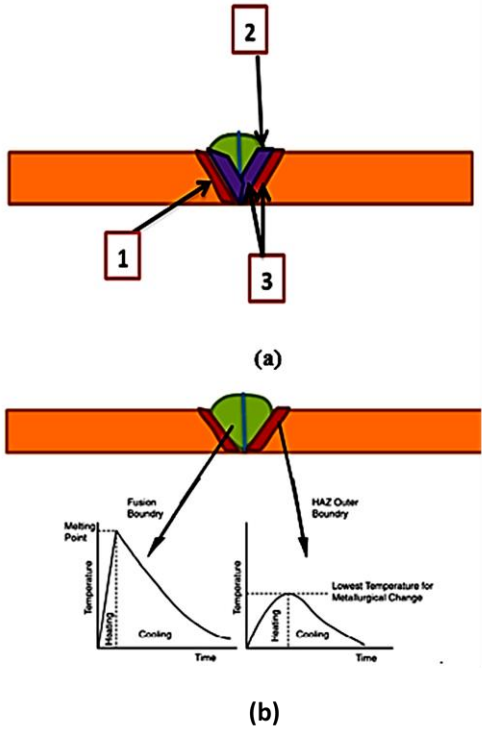

Fig. 8 a) Schematic section of the formed welding zones: {1} sensitive zone (SZ), {2} Heat-affected zone (HAZ), {3} True Heat-affected zone, and b) thermal cycles in weld zones [22].

3.5 Effect of heat input on welded zone

In the area of the welded zone, only dendrites were discovered. Due to the effect of heat input fluctuation on the characterization of dendrites, dendrites affect the mechanical properties of welded joints. When the heat input increases, it has been noticed that the rapid cooling rate leads to a shorter local solidification time and a finer dendrite structure.

Fig. 10 reveals that because of the slow cooling rate, the proper growth of dendrites is visible when the heat input increases. The arms of large dendrites develop during solidification at the expense of those of smaller dendrites.

As demonstrated in Fig. 11, when the cooling rate was sluggish during solidification, more time was available for coarsening, resulting in increased dendritic size and arm spacing. The dendritic spacing slightly decreases at the weld pool's top surface and rises towards the base metal. Because the cooling rate is greater at the top surface of the welding joint and decreases towards the base metal, the consequence mentioned above occurs.

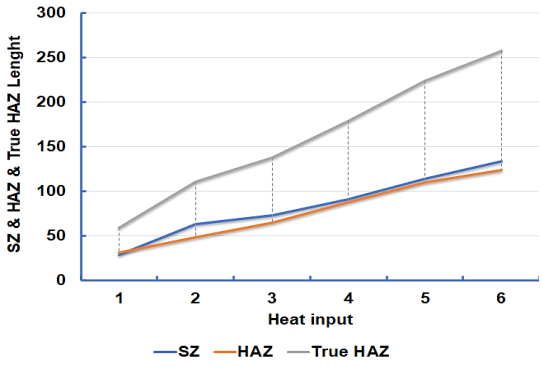

Fig. 9 Effect of different heat inputs on SZ& HAZ & True HAZ Length.

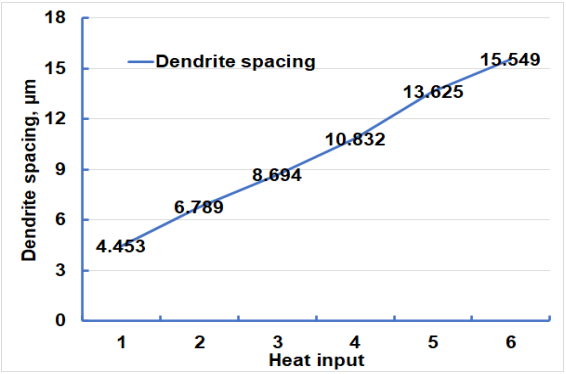

Fig. 11 Effect of heat inputs on dendrite- spacing.

IJMTI vol. 3, issue 2 (2023) 19-29 https://doi.org/10.21608/IJMTI.2023.196160.1078

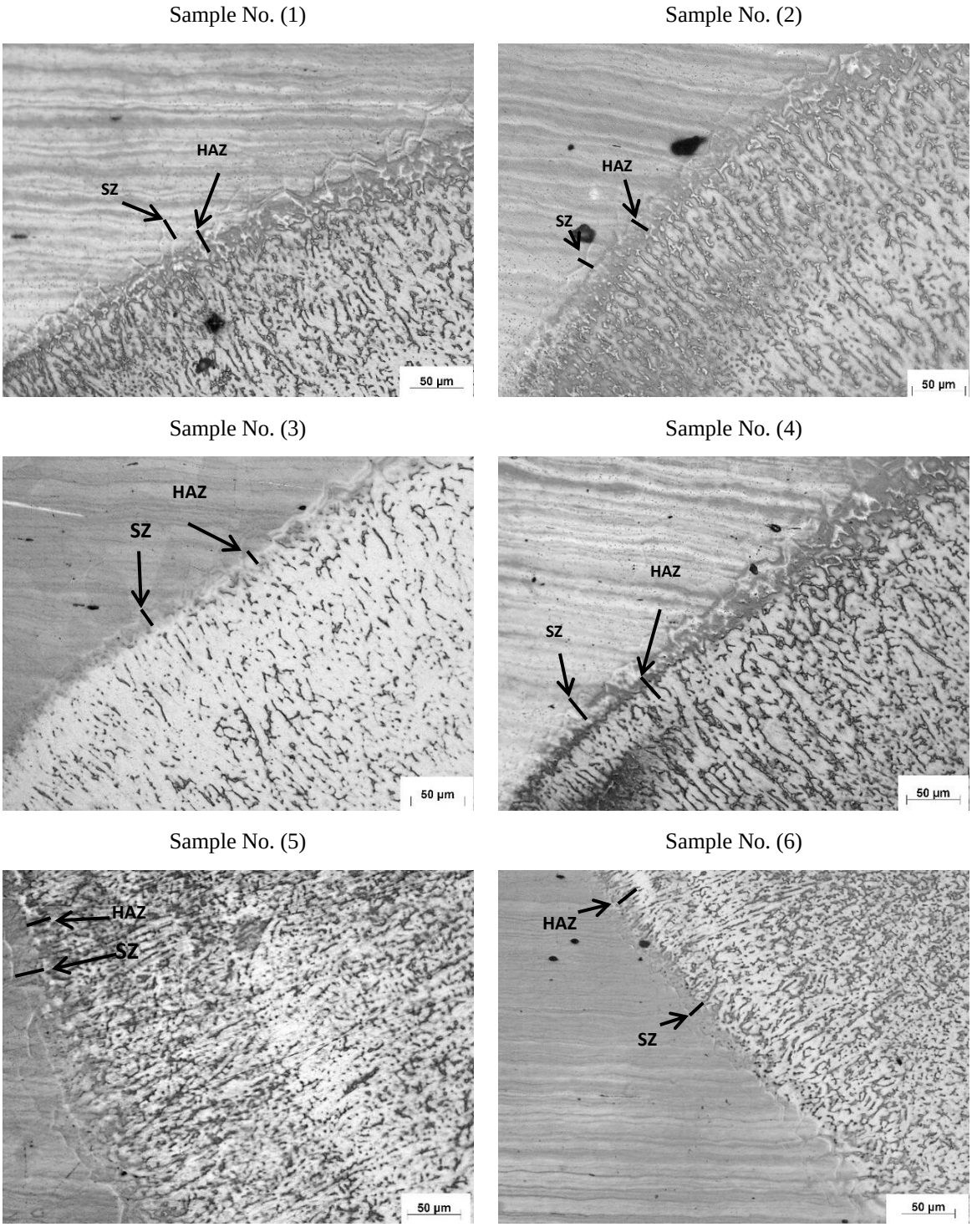

Fig. 10 Effect of heat inputs on HAZ.

IJMTI vol. 3, issue 2 (2023) 19-29 https://doi.org/10.21608/IJMTI.2023.196160.1078

3.6 Tensile properties evaluation

Utilizing the tensile testing machine "Shenzhen WANCE testing machine," tensile strength was determined. Heat input impacts filler material penetration. Reduced heat input in samples 1, 2, and 3 reduces penetration, as seen by the macrostructure analysis in Fig. 6.

Compared to the maximum value attained in a complete penetration sample, the tensile strength value achieved with a partial penetration in the welded zone is lower. Complete penetrations in the welded joints were caused by the high heat input in samples 4, 5, and 6. Sample 4, with its narrower dendrites and lower inter-node spacing, had the full-penetration group's highest ultimate tensile strength (UTS), Table 5.

Table. 5 Effect of heat inputs on ultimate tensile strength

No.	Ultimate tensile strength (MPa)
1	391
2	581
3	772
4	1000
5	885
6	800

The tensile strength of the base material value is equal to 890 MPa. The sample (no 4) is the highest ultimate tensile strength (UTS), and the fracture occurred at the base metal. The previous result approved that the investigated steel (low nickel, high manganese austenitic stainless steel) has good weldability.

3.7 Microhardness measurements

Micro-hardness was measured at a cross-section in the transverse direction perpendicular to the welding fusion line. Table 6 shows the range of hardness in the sample, from low to high heat input. In HAZ, the grains that are partially unmelted in PMZ (partially melted zone which are adopted partially as nuclei during solidification of the welded metal joint) account for the maximum hardness values of 335, 325, 315,310,307, and 293 VHN throughout a range of heat inputs from sample 1 to sample 6. In welded zone (WZ) accounts for the minimum hardness values of 289, 287, 283,278,269, and 262 VHN. These values were compared to the base material value, equal to 290 VHN. The mentioned result approved that the investigated steel (low nickel, high manganese austenitic stainless steel) has good weldability.

Afterward, in the HAZ region, samples show a decreasing trend of hardness because of grain coarsening. In HAZ, a region near PMZ was subjected to a slower cooling rate, resulting in coarse grains, whereas the area towards the base metal having a rapid cooling rate produced a structure with refined grains.

Table. 6 Average microhardness readings in HAZ & WZ

No.	Average of microhardness in HAZ (VHN)	Average of microhardness in WZ (VHN)
1	335	289
2	325	287
3	315	283
4	310	278
5	307	269
6	293	262

IJMTI vol. 3, issue 2 (2023) 19-29 https://doi.org/10.21608/IJMTI.2023.196160.1078

Sample No. (1)

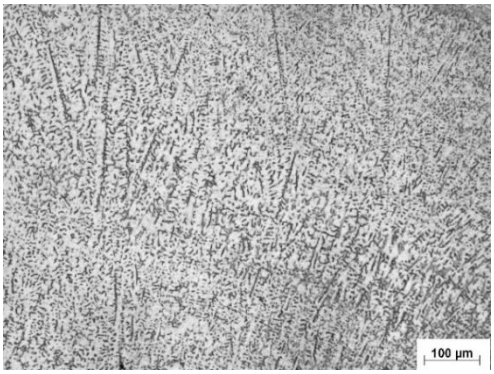

Sample No. (2)

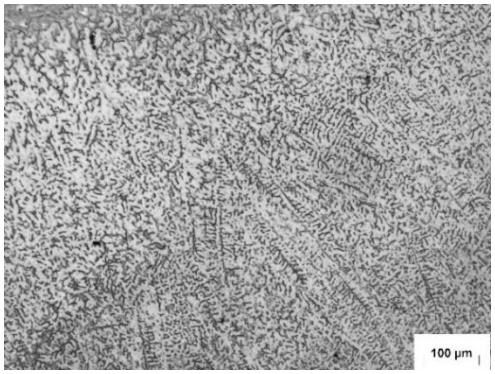

Sample No. (3)

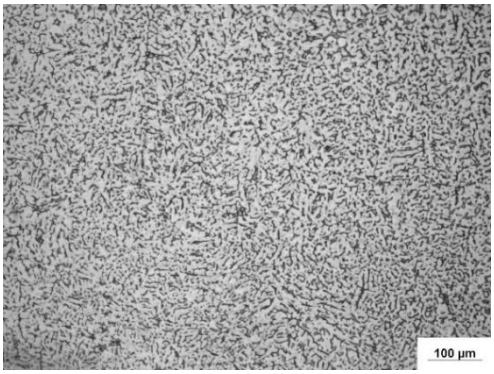

Sample No. (4)

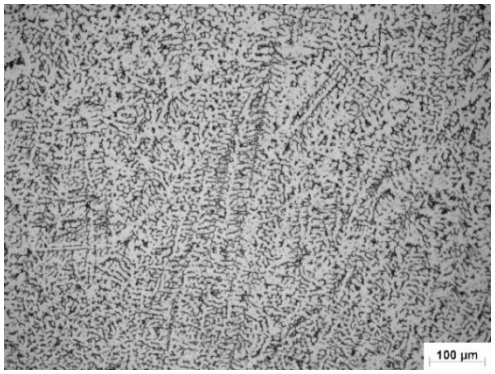

Sample No. (5)

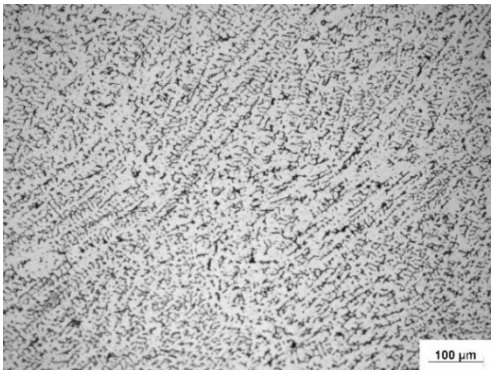

Sample No. (6)

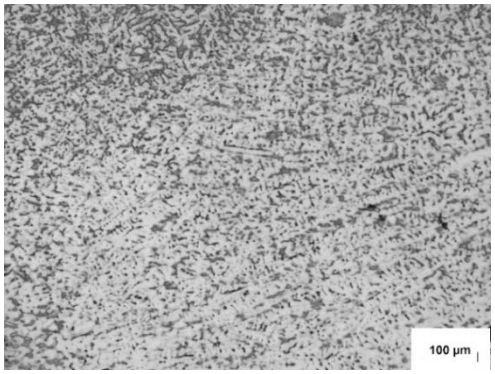

Fig. 12 Effect of heat input on the dendritic structure of the welded zone.

IJMTI vol. 3, issue 2 (2023) 19-29 https://doi.org/10.21608/IJMTI.2023.196160.1078

4. Conclusions

The results of the present study concerning the influence of heat input on the microstructure and mechanical properties of welded high manganese low-nickel stainless steel are as follows:

1. The investigated base steel microstructures consisted of austenite-martensite phases 45-55%, respectively.
2. Heat input increases the dilution in the welding zone, consequently increasing the measured ferrite number.
3. Increases in heat inputs increase the width of heat affected zone. Accordingly, there are significant variations in grain size (coarsening) and HAZ growth.
4. By optimum heat input value (the lowest heat input that achieves full penetration), maximum tensile strength is obtained in smaller dendrites and low spacing of the welded metal joint.
5. The hardness profile shows different trends because of PMZ formation (at partially un-melted regions, hardness is very high).
6. Heat input had a more significant influence on the tensile strength, and it is observed that tensile strength reduced with an increase in heat input and testing temperatures.
7. It is recommended to select parameters that would result in optimum δ- ferrite content in the weld as it influences the mechanical properties of the weld.

References

[1] Brook Hunt: Nickel in perspective, Wood Mackenzie Ltd, January (2010).

[2] M. Amitava, P.K. De, D.K. Bhattacharya, P.K. Srivastava, D.C. Jiles, Ferromagnetic properties of deformation-induced martensite transformation in AISI 304 stainless steel. Metall. Mater. Trans. A 35, 599–605 (2004). https://link.springer.com/article/10.1007/s11661-004-0371-6

[3] J.P. Schille, Z. Guo, N. Saunders, A.P. Miodownik, Modeling phase transformations and material properties critical to processing simulation of steels. Mater. Manuf. Process. 26, 137– 143 (2011) https://www.tandfonline.com/doi/abs/10.1080/10426910903153059

[4] "New 200-series" Steels: An Opportunity or A Threat to the Image of Stainless Steel? ISSF, Brussels, Belgium, (2005). file:///C:/Users/Pc/Downloads/European_200_Sereies_EN%20(1).pdf

[5] S. S. M. Tavares, J. M. Pardal, M. J. Gomes da silva, H. F. G. Abreu and M. R. da silva: Mater. Charact, 60, No. 8, 907, (2009).

[6] N. Nakada, N. Hirakawa, T. Tsuchiyama, S. Takaki, Grain refinement of nickel-free high nitrogen austenitic stainless steel by reversion of eutectoid structure. Scr. Mater. 57, 153–156 (2007). https://www.sciencedirect.com/science/article/abs/pii/S1359646207002060

[7] T. Masumura, N. Nakada, T. Tsuchiyama, S. Takaki, T. Koyano, K. Adachi, The difference in thermal and mechanical stabilities of austenite between carbon and nitrogen-added metastable austenitic stainless steels. Acta Mater.84, 330–338 (2015). https://www.sciencedirect.com/science/article/abs/pii/S1359645414008052

[8] Y. Fu, X. Wu, E.N. Han, W. Ke, K. Yang, Z. Jiang, Effects of nitrogen on the passivation of nickel-free high nitrogen and manganese stainless steels in acidic chloride solutions. Electro-chem. Acta 54, 4005–4014 (2009) . https://www.sciencedirect.com/science/article/abs/pii/S0013468609002606

[9] Valtair Antonio Ferraresi and AmericoScotti: Quality and cost approach for welding process selection, Journal of the Brazilian Society of Mechanical Science, January 2000. https://www.researchgate.net/publication/26354225_Quality_and_cost_approach_for_welding_process_selection

[10] J. C. Lippold and D. J. Kotecki: Welding Metallurgy and Weldability of Stainless Steels, John Wiley & Sons Inc. U.K., (2005) https://www.wiley.com/enus/Welding+Metallurgy+and+Weldability+of+Stainless+Steels-p-9780471473794

[11] R.W. Messler, Principles of Welding: Processes, Physics, Chemistry, and Metallurgy. Physiks Textbook, Wiley-VCH, Weinheim, 2004

[12] A. M. S. Hamouda, S. Sulaiman, T. R. Vijayaram, M. Sayuti and M. H. M. Ahmad: J. Achiev. Mater.Manuf. Eng., 25, No. 1, 63, (2007).

[13] Y.-Q. Zhang, H.-Q.Zhang, I.-F. LIU and R. Wei: J. Iron Steel Res., 16, No. 5, 73, (2009).

IJMTI vol. 3, issue 2 (2023) 19-29 https://doi.org/10.21608/IJMTI.2023.196160.1078

[14] N. Arivazhagan, S. Singh, S. Prakash, G.M. Reddy, Investigation on AISI 304austenitic stainless steel to AISI 4140 low alloy steel dissimilar joints by gas tungsten arc, electron beam, and friction

[15] H. Vashishtha, R.V. Taiwade, S. Sharma, A.P. Patil, Effect of welding processes on microstructural and mechanical properties of dissimilar weldments between conventional austenitic and high nitrogen austenitic stainless steels. J. Manuf. Processes. 25, 49–59 (2017)

[16] Y. D. Han, H. Y. Jing, and L. Y. Xu: Mater. Chem. Phys., 132, No. 1, 216, (2012).

[17] L. M. Gourd: Principles of Welding Metallurgy, 1st South Asian ed., A Butterworth-Heinemann, Oxford, (1998).

[18] K. Weman: Welding Processes Handbook, Woodhead Publishing Ltd, New York, (2003)

[19] Standard Tests Methods for Tension Testing of Metallic Materials (Metric), ASTM E 8M, ASTM, Philadelphia, PA, (1989)

[20] F. B. Pickering: The Metallurgical Evolution of Stainless Steel, ASM International, Metals Park, OH, (1979).

[21] D.J. Kotecki, T.A. Sievert, WRC-1992 constitution diagram for stainless steel weld metals: a modification of the WRC-1988 diagram. Weld. J. 71, 171s–178s (1992).

[22] K. Rajasekhar, C.S. Harendranath, R. Raman, S.D. Kulkarni, Microstructural evolution during solidification of austenitic stainless steel weld metals: a color metallographic and electron microprobe analysis study. Mater.Charact.38, 53–65 (1997).

[23] Bringas, Johan E., Thomas, R. David: Metals blue book welding filler material Handbook, fourth edition, Canada, January (2003).